# Application of the Three-Dimensional Finite-Difference Time-Domain Method to the Analysis of Planar Microstrip Circuits

DAVID M. SHEEN, SAMI M. ALI, SENIOR MEMBER, IEEE, MOHAMED D. ABOUZAHRA, SENIOR MEMBER, IEEE, AND JIN AU KONG, FELLOW, IEEE

*Abstract*—**A direct three-dimensional finite-difference time-domain (FDTD) method is applied to the full-wave analysis of various microstrip structures. The method is shown to be an efficient tool for modeling complicated microstrip circuit components as well as microstrip antennas. From the time-domain results, the input impedance of a line-fed rectangular patch antenna and the frequency-dependent scattering parameters of a low-pass filter and a branch line coupler are calculated. These circuits are fabricated and the measurements are compared with the FDTD results and shown to be in good agreement.**

## I. Introduction

FREQUENCY-domain analytical work with complicated microstrip circuits has generally been done using planar circuit concepts in which the substrate is assumed to be thin enough that propagation can be considered in two dimensions by surrounding the microstrip with magnetic walls [1]–[6]. Fringing fields are accounted for by using either static or dynamic effective dimensions and permittivities. Limitations of these methods are that fringing, coupling, and radiation must all be handled empirically since they are not allowed for in the model. Also, the accuracy is questionable when the substrate becomes thick relative to the width of the microstrip. To fully account for these effects, it is necessary to use a full-wave solution.

Full-wave frequency-domain methods have been used to solve some of the simpler discontinuity problems [7], [8]. However, these methods are difficult to apply to a typical printed microstrip circuit.

Modeling of microstrip circuits has also been performed using Bergeron's method [9], [10]. This method is a modification of the transmission line matrix (TLM) method, and has limitations similar to the finite-difference time-domain (FDTD) method due to the discrete modeling of space and time [11], [12]. A unique problem with this method is that the dielectric interface and the perfectly conducting strip are misaligned by half a space step [12].

The FDTD method has been used extensively for the solution of two- and three-dimensional scattering problems [13]–[17]. Recently, FDTD methods have been used to effectively calculate the frequency-dependent characteristics of microstrip discontinuities [18]–[21]. Analysis of the fundamental discontinuities is of great importance since more complicated circuits can be realized by interconnecting microstrip lines with these discontinuities and using transmission line and network theory. Some circuits, however, such as patch antennas, may not be realized in this way. Additionally, if the discontinuities are too close to each other the use of network concepts will not be accurate due to the interaction of evanescent waves. To accurately analyze these types of structures it is necessary to simulate the entire structure in one computation. The FDTD method shows great promise in its flexibility in handling a variety of circuit configurations. An additional benefit of the time-domain analysis is that a broad-band pulse may be used as the excitation and the frequency-domain parameters may be calculated over the entire frequency range of interest by Fourier transform of the transient results.

In this paper, the frequency-dependent scattering parameters have been calculated for several printed microstrip circuits, specifically a line-fed rectangular patch antenna, a low-pass filter, and a rectangular branch line coupler. These circuits represent resonant microstrip structures on an open substrate; hence, radiation effects can be significant, especially for the microstrip antenna. Calculated results are presented and compared with experimental measurements.

The FDTD method has been chosen over the other discrete methods (TLM or Bergeron's) because it is extremely efficient, its implementation is quite straightforward, and it may be derived directly from Maxwell's equations. Many of the techniques used to implement this

Manuscript received September 29, 1989; revised March 21, 1990. This work was supported by NSF Grant 8620029-ECS, the Joint Services Electronics Program (Contract DAAL03-89-C-0001), RADC Contract F19628-88-K-0013, ARO Contract DAAL03-88-J-0057, ONR Contract N00014-89-J-1019, and the Department of the Air Force.

D. M. Sheen, S. M. Ali, and J. A. Kong are with the Department of Electrical Engineering and Computer Science and the Research Laboratory of Electronics, Massachusetts Institute of Technology, Cambridge, MA 02139.

M. D. Abouzahra is with MIT Lincoln Laboratory, Lexington, MA 02173.

IEEE Log Number 9036153.

method have been demonstrated previously [18]–[20]; however, simplification of the method has been achieved by using a simpler absorbing boundary condition [22]. This simpler absorbing boundary condition yields good results for the broad class of microstrip circuits considered by this paper. Additionally, the source treatment has been enhanced to reduce the source effects documented in [18]–[20].

## II. Problem Formulation

The FDTD method is formulated by discretizing Maxwell's curl equations over a finite volume and approximating the derivatives with centered difference approximations. Conducting surfaces are treated by setting tangential electric field components to 0. The walls of the mesh, however, require special treatment to prevent reflections from the mesh termination.

### A. Governing Equations

Formulation of the FDTD method begins by considering the differential form of Maxwell's two curl equations which govern the propagation of fields in the structures. For simplicity, the media are assumed to be piecewise uniform, isotropic, and homogeneous. The structure is assumed to be lossless (i.e., no volume currents or finite conductivity). With these assumptions, Maxwell's curl equations may be written as

$$\mu \frac{\partial \boldsymbol{H}}{\partial t} = -\nabla \times \boldsymbol{E} \tag{1}$$

$$\epsilon \frac{\partial \boldsymbol{E}}{\partial t} = \nabla \times \boldsymbol{H}. \tag{2}$$

In order to find an approximate solution to this set of equations, the problem is discretized over a finite three-dimensional computational domain with appropriate boundary conditions enforced on the source, conductors, and mesh walls.

### B. Finite-Difference Equations

To obtain discrete approximations to these continuous partial differential equations the centered difference approximation is used on both the time and space first-order partial differentiations. For convenience, the six field locations are considered to be interleaved in space as shown in Fig. 1, which is a drawing of the FDTD unit cell [13]. The entire computational domain is obtained by stacking these rectangular cubes into a larger rectangular volume. The $\hat{x}$, $\hat{y}$, and $\hat{z}$ dimensions of the unit cell are $\Delta x$, $\Delta y$, and $\Delta z$, respectively. The advantages of this field arrangement are that centered differences are realized in the calculation of each field component and that continuity of tangential field components is automatically satisfied. Because there are only six unique field components within the unit cell, the six field components touching the shaded upper eighth of the unit cell in Fig. 1 are considered to be a unit node with subscript indices $i$, $j$, and $k$ corresponding to the node numbers in the $\hat{x}$, $\hat{y}$, and $\hat{z}$ directions. This notation implicitly assumes the $\pm 1/2$ space indices and thus simplifies the notation, rendering the formulas directly implementable on the computer. The time steps are indicated with the superscript $n$. Using this field component arrangement, the above notation, and the centered difference approximation, the explicit finite difference approximations to (1) and (2) are

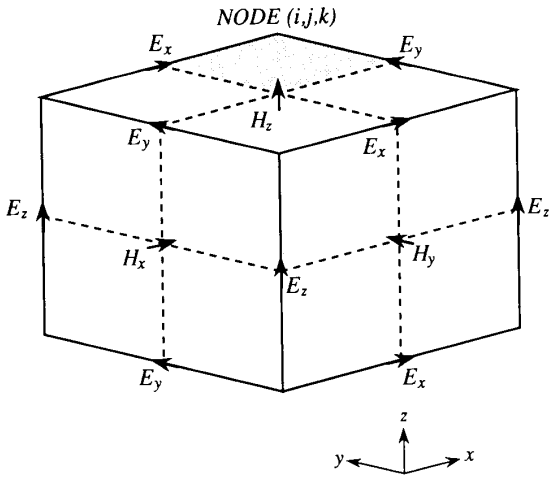


Fig. 1. Field component placement in the FDTD unit cell.

$$H^{n+1/2}_{x\,i,j,k} = H^{n-1/2}_{x\,i,j,k} + \frac{\Delta t}{\mu\,\Delta z}\left(E^{n}_{y\,i,j,k} - E^{n}_{y\,i,j,k-1}\right) - \frac{\Delta t}{\mu\,\Delta y}\left(E^{n}_{z\,i,j,k} - E^{n}_{z\,i,j-1,k}\right) \tag{3}$$

$$H^{n+1/2}_{y\,i,j,k} = H^{n-1/2}_{y\,i,j,k} + \frac{\Delta t}{\mu\,\Delta x}\left(E^{n}_{z\,i,j,k} - E^{n}_{z\,i-1,j,k}\right) - \frac{\Delta t}{\mu\,\Delta z}\left(E^{n}_{x\,i,j,k} - E^{n}_{x\,i,j,k-1}\right) \tag{4}$$

$$H^{n+1/2}_{z\,i,j,k} = H^{n-1/2}_{z\,i,j,k} + \frac{\Delta t}{\mu\,\Delta y}\left(E^{n}_{x\,i,j,k} - E^{n}_{x\,i,j-1,k}\right) - \frac{\Delta t}{\mu\,\Delta x}\left(E^{n}_{y\,i,j,k} - E^{n}_{y\,i-1,j,k}\right) \tag{5}$$

$$E^{n+1}_{x\,i,j,k} = E^{n}_{x\,i,j,k} + \frac{\Delta t}{\epsilon\,\Delta y}\left(H^{n+1/2}_{z\,i,j+1,k} - H^{n+1/2}_{z\,i,j,k}\right) - \frac{\Delta t}{\epsilon\,\Delta z}\left(H^{n+1/2}_{y\,i,j,k+1} - H^{n+1/2}_{y\,i,j,k}\right) \tag{6}$$

$$E^{n+1}_{y\,i,j,k} = E^{n}_{y\,i,j,k} + \frac{\Delta t}{\epsilon\,\Delta z}\left(H^{n+1/2}_{x\,i,j,k+1} - H^{n+1/2}_{x\,i,j,k}\right) - \frac{\Delta t}{\epsilon\,\Delta x}\left(H^{n+1/2}_{z\,i+1,j,k} - H^{n+1/2}_{z\,i,j,k}\right) \tag{7}$$

$$E^{n+1}_{z\,i,j,k} = E^{n}_{z\,i,j,k} + \frac{\Delta t}{\epsilon\,\Delta x}\left(H^{n+1/2}_{y\,i+1,j,k} - H^{n+1/2}_{y\,i,j,k}\right) - \frac{\Delta t}{\epsilon\,\Delta y}\left(H^{n+1/2}_{x\,i,j+1,k} - H^{n+1/2}_{x\,i,j,k}\right). \tag{8}$$

The half time steps indicate that $\boldsymbol{E}$ and $\boldsymbol{H}$ are alternately calculated in order to achieve centered differences for the time derivatives. In these equations, the permittivity and the permeability are set to the appropriate values depending on the location of each field component. For the electric field components on the dielectric–air interface the average of the two permittivities, $(\epsilon_0 + \epsilon_1)/2$, is used. The validity of this treatment is explained in [20].

Due to the use of centered differences in these approximations, the error is second order in both the space and time steps; i.e., if $\Delta x$, $\Delta y$, $\Delta z$, and $\Delta t$ are proportional to $\Delta l$, then the global error is $O(\Delta l^2)$. The maximum time step that may be used is limited by the stability restriction of the finite difference equations,

$$\Delta t \leq \frac{1}{v_{\max}} \left( \frac{1}{\Delta x^2} + \frac{1}{\Delta y^2} + \frac{1}{\Delta z^2} \right)^{-1/2} \tag{9}$$

where $v_{\max}$ is the maximum velocity of light in the computational volume. Typically, $v_{\max}$ will be the velocity of light in free space unless the entire volume is filled with dielectric. These equations will allow the approximate solution of $\boldsymbol{E}(\boldsymbol{r},t)$ and $\boldsymbol{H}(\boldsymbol{r},t)$ in the volume of the computational domain or mesh; however, special consideration is required for the source, the conductors, and the mesh walls.

### C. Source Considerations

The volume in which the microstrip circuit simulation is to be performed is shown schematically in Fig. 2. At $t = 0$ the fields are assumed to be identically 0 throughout the computational domain. A Gaussian pulse is desirable as the excitation because its frequency spectrum is also Gaussian and will therefore provide frequency-domain information from dc to the desired cutoff frequency by adjusting the width of the pulse.

In order to simulate a voltage source excitation it is necessary to impose the vertical electric field, $E_z$, in a rectangular region underneath port 1 as shown in Fig. 2. The remaining electric field components on the source plane must be specified or calculated. In [18]–[20] an electric wall source is used; i.e., the remaining electric field components on the source wall of the mesh are set to 0. An unwanted side effect of this type of excitation is that a sharp magnetic field is induced tangential to the source wall. This results in some distortion of the launched pulse. Specifically, the pulse is reduced in magnitude due to the energy stored in the induced magnetic field and a negative tail to the pulse is immediately evident. An alternative excitation scheme is to simulate a magnetic wall at the source plane. The source plane consists only of $E_x$ and $E_z$ components, with the tangential magnetic field components offset $\pm \Delta y/2$. If the magnetic wall is enforced by setting the tangential magnetic field components to zero just behind the source plane, then significant distortion of the pulse still occurs. If the magnetic wall is enforced directly on the source plane by using image theory (i.e., $\boldsymbol{H}_{\tan}$ outside the magnetic wall is equal to $-\boldsymbol{H}_{\tan}$ inside the magnetic wall), then the remaining electric field components on the source plane may be readily calculated using the finite-difference equations. Using this excitation, only a minimal amount of source distortion is apparent. The launched wave has nearly unit amplitude and is Gaussian in time and in the $\hat{y}$ direction:

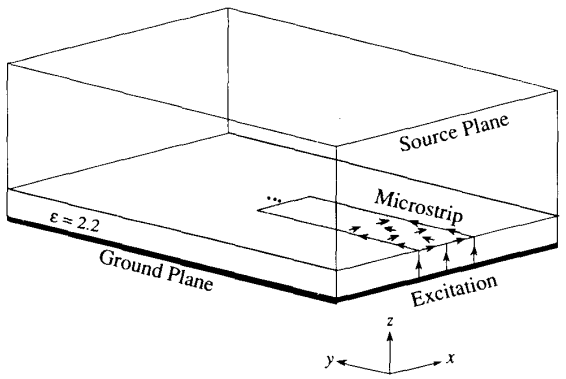


Fig. 2. Computational domain.

$$E_z = f_s(t) = e^{-(t-t_0)^2/T^2}. \tag{10}$$

It is assumed that excitation specified in this way will result in the fundamental mode only propagating down the microstrip in the frequency range of interest.

The finite-difference formulas are not perfect in their representation of the propagation of electromagnetic waves. One effect of this is numerical dispersion; i.e., the velocity of propagation is slightly frequency dependent even for uniform plane waves. In order to minimize the effects of numerical dispersion and truncation errors, the width of the Gaussian pulse is chosen for at least 20 points per wavelength at the highest frequency represented significantly in the pulse.

### D. Conductor Treatment

The circuits considered in this paper have a conducting ground plane and a single dielectric substrate with metallization on top of this substrate in the ordinary microstrip configuration. These electric conductors are assumed to be perfectly conducting and have zero thickness and are treated by setting the electric field components that lie on the conductors to zero. The edge of the conductor should be modeled with electric field components tangential to the edge lying exactly on the edge of the microstrip as shown in Fig. 2.

### E. Absorbing Boundary Treatment

Due to the finite capabilities of the computers used to implement the finite-difference equations, the mesh must be limited in the $\hat{x}$, $\hat{y}$, and $\hat{z}$ directions. The difference equations cannot be used to evaluate the field components tangential to the outer boundaries since they would require the values of field components outside of the mesh. One of the six mesh boundaries is a ground plane and its tangential electric field values are forced to be 0.

The tangential electric field components on the other five mesh walls must be specified in such a way that outgoing waves are not reflected using the absorbing boundary condition [22], [23]. For the structures considered in this paper, the pulses on the microstrip lines will be normally incident to the mesh walls. This leads to a simple approximate continuous absorbing boundary condition, which is that the tangential fields on the outer boundaries will obey the one-dimensional wave equation in the direction normal to the mesh wall. For the $\hat{y}$ normal wall the one-dimensional wave equation may be written

$$\left(\frac{\partial}{\partial y} - \frac{1}{v}\frac{\partial}{\partial t}\right) \boldsymbol{E}_{\tan} = 0. \tag{11}$$

This equation is Mur's first approximate absorbing boundary condition and it may be easily discretized using only field components on or just inside the mesh wall, yielding an explicit finite difference equation [22],

$$E_0^{n+1} = E_1^n + \frac{v\Delta t - \Delta y}{v\Delta t + \Delta y}\left(E_1^{n+1} - E_0^n\right) \tag{12}$$

where $E_0$ represents the tangential electric field components on the mesh wall and $E_1$ represents the tangential electric field components one node inside of the mesh wall. Similar expressions are immediately obtained for the other absorbing boundaries by using the corresponding normal directions for each wall. It should be noted that the normal incidence assumption is not valid for the fringing fields which are propagating tangential to the walls; therefore the sidewalls should be far enough away that the fringing fields are negligible at the walls. Additionally, radiation will not be exactly normal to the mesh walls. Second-order absorbing boundary conditions [22], [23] which account for oblique incidence will not work on the mesh walls where the microstrip is incident because these absorbing boundary conditions are derived in uniform space.

The results presented show that the first-order absorbing boundary treatment is sufficiently accurate and particularly well suited to the microstrip geometry. It is possible to obtain more accurate normal incidence absorbing boundary conditions [24], which have been used in the FDTD calculation of microstrip discontinuities [20]. Due to the more dynamic, resonant behavior of the circuits considered, Mur's first approximate absorbing boundary condition is used and this allows for accurate simulation of the various microstrip circuits.

### F. Time Marching Solution

The finite difference equations, (3)–(8), are used with the above boundary and source conditions to simulate the propagation of a broad-band Gaussian pulse on the microstrip structure. The essential aspects of the time-domain algorithm are as follows:

- Initially (at $t = n = 0$) all fields are 0.
- The following are repeated until the response is $\approx 0$:
  Gaussian excitation is imposed on port 1.
  $\boldsymbol{H}^{n+1/2}$ is calculated from FD equations.
  $\boldsymbol{E}^{n+1}$ is calculated from FD equations.
  Tangential $\boldsymbol{E}$ is set to 0 on conductors.
  Save desired field quantities.
  $n \rightarrow n+1$.
- Compute scattering matrix coefficients from time-domain results.

One additional consideration is that the reflections from the circuit will be reflected again by the source wall. To eliminate this, the circuit is placed a sufficient distance from the source, and after the Gaussian pulse has been fully launched, the absorbing boundary condition is switched on at the source wall.

### G. Frequency-Dependent Parameters

In addition to the transient results obtained naturally by the FDTD method, the frequency-dependent scattering matrix coefficients are easily calculated.

$$[V]^r = [S][V]^i \tag{13}$$

where $[V]^r$ and $[V]^i$ are the reflected and incident voltage vectors, respectively, and $[S]$ is the scattering matrix. To accomplish this, the vertical electric field underneath the center of each microstrip port is recorded at every time step. As in [20], it is assumed that this field value is proportional to the voltage (which could be easily obtained by numerically integrating the vertical electric field) when considering propagation of the fundamental mode. To obtain the scattering parameter $S_{11}(\omega)$, the incident and reflected waveforms must be known. The FDTD simulation calculates the sum of incident and reflected waveforms. To obtain the incident waveform, the calculation is performed using only the port 1 microstrip line, which will now be of infinite extent (i.e., from source to far absorbing wall), and the incident waveform is recorded. This incident waveform may now be subtracted from the incident plus reflected waveform to yield the reflected waveform for port 1. The other ports will register only transmitted waveforms and will not need this computation. The scattering parameters, $S_{jk}$, may then be obtained by simple Fourier transform of these transient waveforms as

$$S_{jk}(\omega) = \frac{\mathcal{FT}\{V_j(t)\}}{\mathcal{FT}\{V_k(t)\}}. \tag{14}$$

Note that the reference planes are chosen with enough distance from the circuit discontinuities to eliminate evanescent waves. These distances are included in the definition of the circuit so that no phase correction is performed for the scattering coefficients. For all of the circuits considered, the only unique coefficients are in

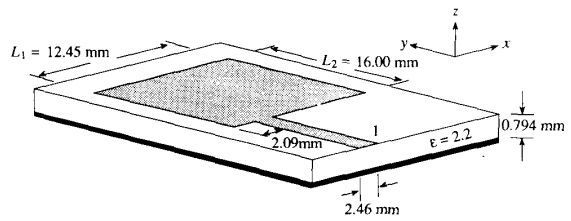


Fig. 3. Line-fed rectangular microstrip antenna detail.

the first column of the scattering matrix (i.e., $S_{11}(\omega), S_{21}(\omega), S_{31}(\omega), \cdots$).

## III. Numerical Results

Numerical results have been computed for three configurations, a line-fed rectangular patch antenna, a low-pass filter, and a branch line coupler. These circuits have dimensions on the order of 1 cm, and the frequency range of interest is from dc to 20 GHz. The operating regions of all of these circuits are less than 10 GHz; however, the accuracy of the computed results at higher frequencies is examined. These circuits were constructed on Duroid substrates with $\epsilon = 2.2$ and thickness of 1/32 inch (0.794 mm). Scattering matrix coefficients were measured using an HP 8510 network analyzer, which is calibrated to 18 GHz, but provides measurement to 20 GHz.

### *A. Line-Fed Rectangular Microstrip Antenna*

The actual dimensions of the microstrip antenna analyzed are shown in Fig. 3. The operating resonance approximately corresponds to the frequency where $L_1 = 1.245$ mm $= \lambda/2$. Simulation of this circuit involves the straightforward application of the finite-difference equations, source, and boundary conditions. To model the thickness of the substrate correctly, $\Delta z$ is chosen so that three nodes exactly match the thickness. An additional 13 nodes in the $\hat{z}$ direction are used to model the free space above the substrate. In order to correctly model the dimensions of the antenna, $\Delta x$ and $\Delta y$ have been chosen so that an integral number of nodes will exactly fit the rectangular patch. Unfortunately, this means the port width and placement will be off by a fraction of the space step. The sizes of the space steps are carefully chosen to minimize the effect of this error.

The space steps used are $\Delta x = 0.389$ mm, $\Delta y = 0.400$ mm, and $\Delta z = 0.265$ mm, and the total mesh dimensions are $60 \times 100 \times 16$ in the $\hat{x}$, $\hat{y}$, and $\hat{z}$ directions respectively. The rectangular antenna patch is thus $32\,\Delta x \times 40\,\Delta y$. The length of the microstrip line from the source plane to the edge of the antenna is $50\,\Delta y$, and the reference plane for port 1 is $10\,\Delta y$ from the edge of the patch. The microstrip line width is modeled as $6\,\Delta x$.

The time step used is $\Delta t = 0.441$ ps. The Gaussian half-width is $T = 15$ ps, and the time delay $t_0$ is set to be $3T$ so the Gaussian will start at approximately 0. The simulation is performed for 8000 time steps, somewhat longer than for other circuits, due to the highly resonant behavior of the antenna. The computation time for this circuit is approximately 12 h on a VAXstation 3500 workstation.

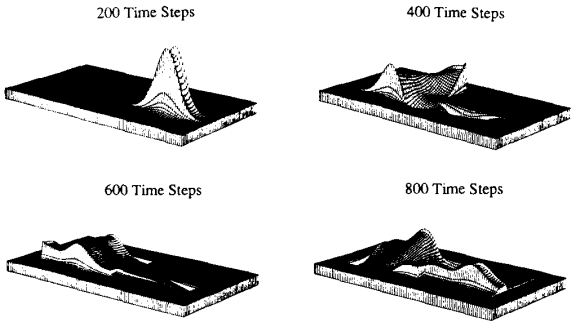


Fig. 4. Rectangular microstrip antenna distribution of $E_z(x, y, t)$ just underneath the dielectric interface at 200, 400, 600, and 800 time steps.

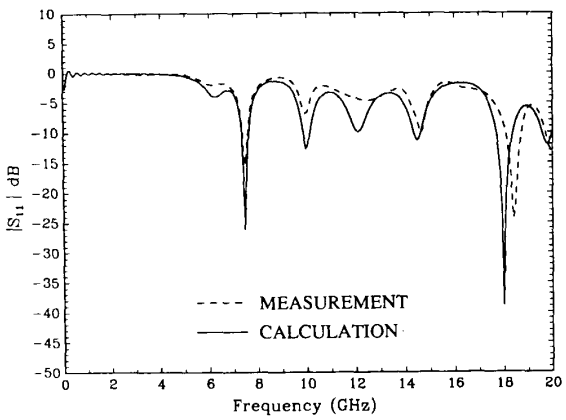


Fig. 5. Return loss of the rectangular antenna.

The spatial distribution of $E_z(x, y, t)$ just beneath the microstrip at 200, 400, 600, and 800 time steps is shown in Fig. 4, where the source Gaussian pulse and subsequent propagation on the antenna are observed. Notice that the absorbing boundary condition for the source has been implemented several nodes from the source plane to eliminate any undesirable effects of switching from source to absorbing boundary conditions. Three-dimensional properties of the propagation are observed including enhancement of the field near the edges of the microstrip.

The scattering coefficient results, shown in Fig. 5, show good agreement with the measured data. The operating resonance at 7.5 GHz is almost exactly shown by both theory and measurement. This result is a significant advancement over planar circuit techniques, which without empirical treatment will allow only $|S_{11}| = 1.0$ because they do not allow for radiation. Also, the resonance frequency calculated using planar circuit concepts will be sensitive to errors in the effective dimensions of the patch. Additional resonances are also in good ageement with experiment, except for the highest resonance near 18 GHz, which is somewhat shifted.

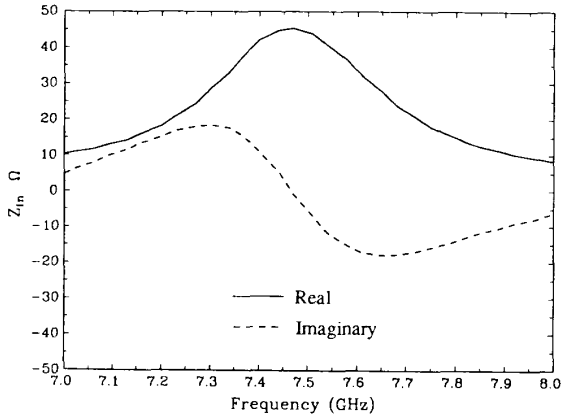


Fig. 6. Input impedance of the rectangular antenna near the operating resonance of 7.5 GHz as calculated from the FDTD results.

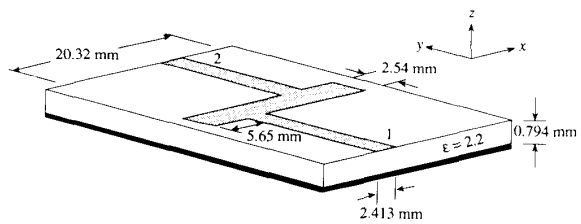


Fig. 7. Low-pass filter detail.

Input impedance for the antenna may be calculated from the $S_{11}(\omega)$ calculation by transforming the reference plane to the edge of the microstrip antenna,

$$Z_{\text{in}} = Z_0 \frac{1 + S_{11} e^{j2kL}}{1 - S_{11} e^{j2kL}} \tag{15}$$

where $k$ is the wavenumber on the microstrip, $L$ is the length from the edge of the antenna to the reference plane ($10\Delta y$), and $Z_0$ is the characteristic impedance of the microstrip line. For simplicity of the $Z_{\text{in}}$ calculation, the microstrip is assumed to have a constant characteristic impedance of 50 Ω, and an effective permittivity of 1.9 is used to calculate the wavenumber. Results for the input impedance calculation near the operating resonance of 7.5 GHz are shown in Fig. 6.

### B. Microstrip Low-Pass Filter

The low-pass filter analyzed is one designed according to the criteria established by [2] and is shown in Fig. 7. As in the rectangular antenna, $\Delta x$, $\Delta y$, and $\Delta z$ are carefully chosen to fit the dimensions of the circuit. The space steps $\Delta x$ and $\Delta y$ are chosen to exactly match the dimensions of the rectangular patch; however, the locations and widths of the ports will be modeled with some error.

The space steps used are $\Delta x = 0.4064$ mm, $\Delta y = 0.4233$ mm, and $\Delta z = 0.265$ mm, and the total mesh dimensions are $80 \times 100 \times 16$ in the $\hat{x}$, $\hat{y}$, and $\hat{z}$ directions respectively. The long rectangular patch is thus $50\Delta x \times 6\Delta y$. The distance from the source plane to the edge of the long patch is $50\Delta y$, and the reference planes for ports 1 and 2 are $10\Delta y$ from the edges of the patch. The strip widths of ports 1 and 2 are modeled as $6\Delta x$.

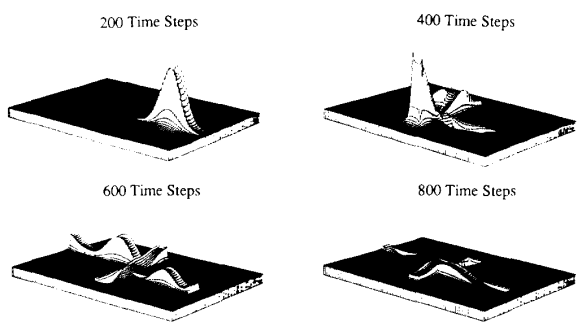


Fig. 8. Low-pass filter distribution of $E_z(x, y, t)$ just underneath the dielectric interface at 200, 400, 600, and 800 time steps.

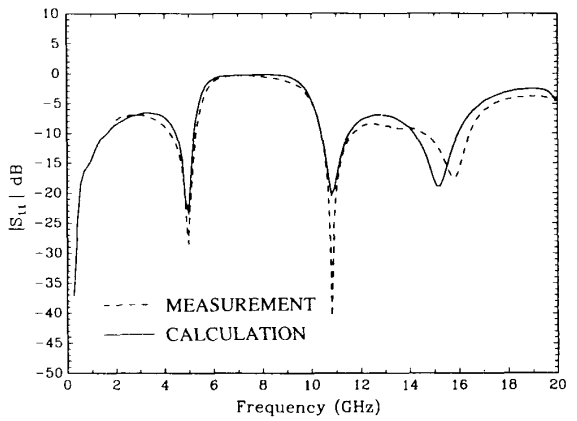


Fig. 9. Return loss of the low-pass filter.

The time step used is $\Delta t = 0.441$ ps. The Gaussian half-width is $T = 15$ ps and the time delay $t_0$ is set to be $3T$. The simulation is performed for 4000 time steps to allow the response on both ports to become nearly 0. The computation time for this circuit is approximately 8 h on a VAXstation 3500 workstation.

The spatial distribution of $E_z(x, y, t)$ just beneath the microstrip at 200, 400, 600, and 800 time steps is shown in Fig. 8. The scattering coefficient results, shown in Figs. 9 and 10, again show good agreement in the location of the response nulls. The desired low-pass filter performance is seen in the sharp $S_{21}$ roll-off beginning at approximately 5 GHz. There is again some shift near the high end of the frequency range. In the $S_{21}$ results, the stopband for the calculated curve is somewhat narrower than the measured results. Some experimentation with planar circuit techniques has led to the conclusion that this narrowing is caused predominantly by the slight misplacement of the ports inherent in the choice of $\Delta x$ and $\Delta y$.

### C. Microstrip Branch Line Coupler

The branch line coupler, shown in Fig. 11, is used to divide power equally between ports 3 and 4 from ports 1 or 2. This occurs at the frequency where the center-to-center distance between the four lines is a quarter wave-

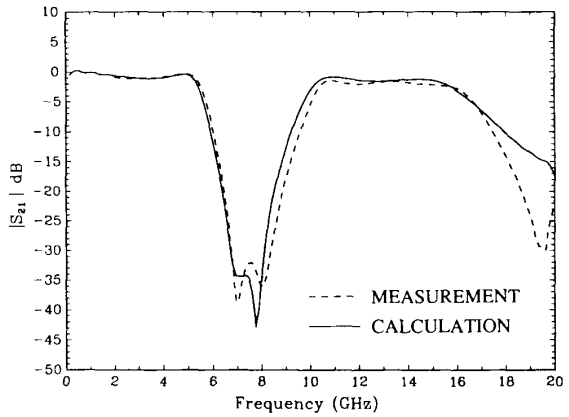


Fig. 10. Insertion loss of the low-pass filter.

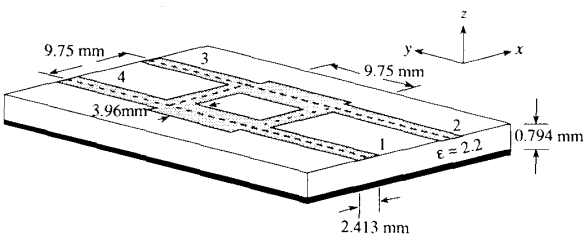


Fig. 11. Branch line coupler detail.

length. Also, the phase difference between ports 3 and 4 is 90° at this frequency. To model this circuit, $\Delta x$, $\Delta y$, and $\Delta z$ are chosen to match the dimensions of the circuit as effectively as possible. The space step, $\Delta z$, is chosen to match the substrate thickness exactly. The space steps, $\Delta x$ and $\Delta y$, are chosen to match the center-to-center distance (9.75 mm) exactly. Again, small errors in the other $\hat{x}$ and $\hat{y}$ dimensions occur.

The space steps used are $\Delta x = 0.406$ mm, $\Delta y = 0.406$ mm, and $\Delta z = 0.265$ mm and the total mesh dimensions are $60 \times 100 \times 16$ in the $\hat{x}$, $\hat{y}$, and $\hat{z}$ directions, respectively. The center-to-center distances are $24\Delta x$ and $24\Delta y$. The distance from the source plane to the edge of the coupler is $50\Delta y$, and the reference planes for ports 1 through 4 are $10\Delta y$ from the edges of the coupler. The strip widths of ports 1 through 4 are modeled as $6\Delta x$. The wide strips in the coupler are modeled as $10\Delta x$ wide.

The time step used is $\Delta t = 0.441$ ps. The Gaussian half-width is $T = 15$ ps and the time delay $t_0$ is set to be $3T$. The simulation is performed for 4000 time steps to allow the response on all four ports to become nearly zero. The computation time for this circuit is approximately 6 h on a VAXstation 3500 workstation.

The spatial distribution of $E_z(x, y, t)$ just beneath the microstrip at 200, 400, 600, and 800 time steps is shown in Fig. 12. The scattering coefficient results, shown in Fig. 13, again show good agreement in the location of the response nulls and crossover point. The desired branch line coupler performance is seen in the sharp $S_{11}$ and $S_{21}$ nulls which occur at approximately the same point (6.5

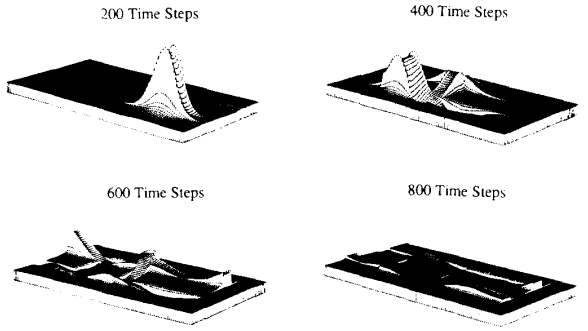


Fig. 12. Branch line coupler distribution of $E_z(x, y, t)$ just underneath the dielectric interface at 200, 400, 600, and 800 time steps.

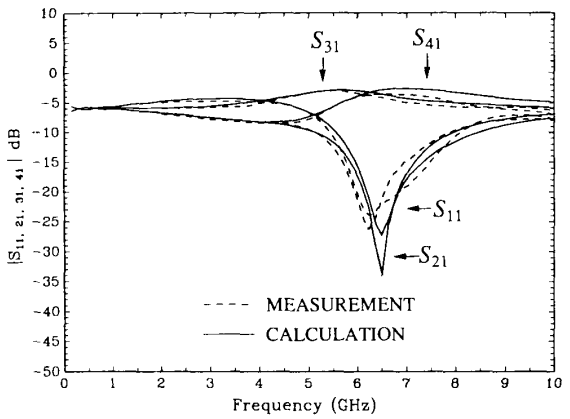


Fig. 13. Scattering parameters of the branch line coupler.

GHz) as the crossover in $S_{31}$ and $S_{41}$. At this crossover point $S_{31}$ and $S_{41}$ are both approximately $-3$ dB, indicating that the power is being evenly divided between ports 3 and 4. The nulls in $S_{11}$ and $S_{21}$ at the operating point indicate that little power is being transmitted by ports 1 and 2. The phase difference between $S_{31}$ and $S_{41}$ is verified to be approximately 90° at the operating point ($\approx 6.5$ GHz) in both the calculated and measured coefficients, as shown in Fig. 14. Some shift in the location of the nulls is again observed and is likely due to the slight modeling errors in the widths of the lines.

### *D. Error Discussion*

In general, agreement between measured and calculated results has been good; however, there are several reasons to explain the small discrepancies in the results. The modeling error occurs primarily in the inability to match all of the circuit dimensions. The space steps, $\Delta x$, $\Delta y$, and $\Delta z$, may be freely chosen; this allows exact matching of only one circuit dimension (or two edges) in each of the $\hat{x}$, $\hat{y}$, and $\hat{z}$ directions. Another small source of error is the exclusion of dielectric and conductor loss in the FDTD calculation. This causes the calculated $S$ parameters to be shifted up in amplitude from the measured data at the higher frequencies. Measurement errors occur because of the microstrip-to-coaxial transitions, which are

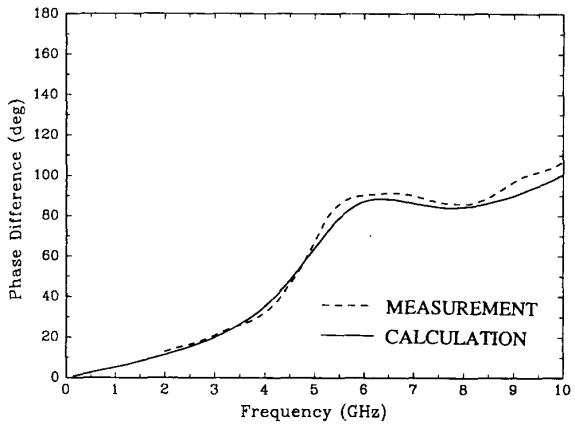


Fig. 14. Phase difference of port 3 relative to port 4 of the branch line coupler.

not de-embedded in the measurement, and because the network analyzer and its connectors are rated only to 18 GHz.

## IV. Conclusions

The finite-difference time-domain method has been used to perform time-domain simulations of pulse propagation in several printed microstrip circuits. In addition to the transient results, frequency-dependent scattering parameters and the input impedance of a line-fed rectangular patch antenna have been calculated by Fourier transform of the time-domain results. These results have been verified by comparison with measured data. The versatility of the FDTD method allows easy calculation of many complicated microstrip structures. With the computational power of computers increasing rapidly, this method is very promising for the computer-aided design of many types of microstrip circuit components.

## References

[1] G. D'Inzeo, F. Giannini, C. Sodi, and R. Sorrentino, "Method of analysis and filtering properties of microwave planar networks," *IEEE Trans. Microwave Theory Tech.*, vol. MTT-26, pp. 462–471, July 1978.

[2] G. D'Inzeo, F. Giannini, and R. Sorrentino, "Novel microwave integrated low-pass filters," *Electron. Lett.*, vol. 15, no. 9, pp. 258–260, Apr. 26, 1979.

[3] K. C. Gupta, R. Garg, and R. Chadha, *Computer-Aided Design of Microwave Circuits*. Dedham, MA: Artech House, 1981.

[4] T. Okoshi, *Planar Circuits for Microwaves and Lightwaves*. Berlin: Springer-Verlag, 1985.

[5] W. K. Gwarek, "Analysis of arbitrarily shaped two-dimensional microwave circuits by finite difference time domain method," *IEEE Trans. Microwave Theory Tech.*, vol. 36, pp. 738–744, Apr. 1988.

[6] K. C. Gupta and M. D. Abouzahra, "Planar circuit analysis," in *Numerical Techniques for Microwave and Millimeter-Wave Passive Structures*, T. Itoh, Ed. New York: Wiley, 1989, pp. 214–333.

[7] P. B. Katehi and N. C. Alexopoulos, "Frequency dependent characteristics of microstrip discontinuities in millimeter wave integrated circuits," *IEEE Trans. Microwave Theory Tech.*, vol. MTT-33, pp. 1029–1035, Oct. 1985.

[8] R. W. Jackson, "Full-wave, finite element analysis of irregular microstrip discontinuities," *IEEE Trans. Microwave Theory Tech.*, vol. 37, pp. 81–89, Jan. 1989.

[9] S. Koike, N. Yoshida, and I. Fukai, "Transient analysis of microstrip line on anisotropic substrate in three-dimensional space," *IEEE Trans. Microwave Theory Tech.*, vol. 36, pp. 34–43, Jan. 1988.

[10] T. Shibata, T. Hayashi, and T. Kimura, "Analysis of microstrip circuits using three-dimensional full-wave electromagnetic field analysis in the time domain," *IEEE Trans. Microwave Theory Tech.*, vol. 36, pp. 1064–1070, June 1988.

[11] S. Akhtarzad and P. B. Johns, "Solution of Maxwell's equations in three space dimensions and time by the T. L. M. method of numerical analysis," *Proc. Inst. Elec. Eng.*, vol. 122, no. 12, pp. 1344–1348, Dec. 1975.

[12] W. J. R. Hoefer, "The transmission-line matrix method—Theory and applications," *IEEE Trans. Microwave Theory Tech.*, vol. MTT-33, pp. 882–893, Oct. 1985.

[13] K. S. Yee, "Numerical solution of initial boundary value problems involving Maxwell's equations in isotropic media," *IEEE Trans. Antennas Propagat.*, vol. AP-14, pp. 302–307, May 1966.

[14] A. Taflove and M. E. Brodwin, "Numerical solution of steady state electromagnetic scattering problems using the time dependent Maxwell's equations," *IEEE Trans. Microwave Theory Tech.*, vol. MTT-23, pp. 623–630, Aug. 1975.

[15] A. Taflove, "Application of the finite difference time domain method to sinusoidal steady state electromagnetic penetration problems," *IEEE Trans. Electromagn. Compat.* vol. EMC-22, pp. 191–202, Aug. 1980.

[16] A. Taflove and K. R. Umashankar, "The finite difference time domain (FD–TD) method for electromagnetic scattering and interaction problems," *J. Electromagn. Waves and Appl.*, vol. 1, no. 3, pp. 243–267, 1987.

[17] A. C. Cangellaris, C. C. Lin, and K. K. Mei, "Point matched time domain finite element methods for electromagnetic radiation and scattering," *IEEE Trans. Antennas Propagat.*, vol. AP-35, pp. 1160–1173, Oct. 1987.

[18] X. Zhang, J. Fang, K. K. Mei, and Y. Liu, "Calculations of the dispersive characteristics of microstrips by the time-domain finite difference method," *IEEE Trans. Microwave Theory Tech.*, vol. 36, pp. 263–267, Feb. 1988.

[19] X. Zhang and K. K. Mei, "Time domain finite difference approach for the calculation of microstrip open-circuit end effect," *IEEE Trans. Microwave Theory Tech.*, in *IEEE MTT-S Int. Microwave Symp. Dig.*, 1988, pp. 363–366.

[20] X. Zhang and K. K. Mei, "Time domain finite difference approach to the calculation of the frequency dependent characteristics of microstrip discontinuities," *IEEE Trans. Microwave Theory Tech.*, vol. 36, pp. 1775–1787, Dec. 1988.

[21] D. H. Choi and W. J. R. Hoefer, "The finite-difference time-domain method and its application to eigenvalue problems," *IEEE Trans. Microwave Theory Tech.*, vol. MTT-34, pp. 1464–1470, Dec. 1986.

[22] G. Mur, "Absorbing boundary conditions for the finite difference approximation of the time domain electromagnetic field equations," *IEEE Trans. Electromagn. Compat.*, vol. EMC-23, pp. 377–382, Nov. 1981.

[23] B. Enquist and A. Majda, "Absorbing boundary conditions for the numerical simulation of waves," *Math. Comput.*, vol. 31, no. 139, pp. 629–651, July 1977.

[24] K. K. Mei and J. Fang, "A super-absorption boundary algorithm for one dimensional wave equations," submitted to *J. Comput. Phys.*

✠

**David M. Sheen** was born in Richland, WA, on March 6, 1964. He received the B.S. degree in electrical engineering from Washington State University in December 1985 and the M.S. degree in electrical engineering from the Massachusetts Institute of Technology, Cambridge, MA, in September 1988. He is currently studying for the Ph.D. degree in the Department of Electrical Engineering and Computer Science at M.I.T. His research interests are in the areas of microwave engineering and numerical solution of electromagnetic wave propagation problems.

**Sami M. Ali** (M'79–SM'86) was born in Egypt on December 7, 1938. He received the B.S. degree from the Military Technical College, Cairo, Egypt, in 1965, and the Ph.D. degree from the Technical University of Prague, Prague, Czechoslovakia, in 1975, both in electrical engineering.

He joined the Electrical Engineering Department, Military Technical College, Cairo, in 1975. In 1985, he became a Professor and head of the Basic Electrical Engineering Department there. From 1981 to 1982 he was a visiting scientist at the Research Laboratory of Electronics, Massachusetts Institute of Technology, Cambridge, MA. Since 1987, he has again been a visiting scientist there. His current research interests deal with microwave integrated circuits and microstrip antenna applications.

✠

**Mohamed D. Abouzahra** (S'79–M'85–SM'87) was born in Beirut, Lebanon, on June 15, 1953. He received the B.S. degree (with distinction) in electronics and communications from Cairo University, Cairo, Egypt, in 1976 and the M.S. and Ph.D. degrees in electrical engineering from the University of Colorado, Boulder, in 1978 and 1984, respectively.

From 1979 to 1984 he worked as a research and teaching assistant at the University of Colorado, Boulder. Since 1984 he has been a member of the technical staff at the Massachusetts Institute of Technology, Lincoln Laboratory, where he has worked on microstrip line discontinuities, wide-band dielectric directional couplers, and dielectric image lines. He is currently interested in the computer-aided design of microwave and millimeter-wave wide-band planar circuits and in the development of wide-band automated measurement schemes for characterizing composite materials.

Dr. Abouzahra has published over 30 research papers and holds one patent in the microwave area. He also coauthored a chapter in *Numerical Techniques for Microwave and Millimeter Wave Passive Structures* (John Wiley). Dr. Abouzahra is on the editorial board of the IEEE TRANSACTIONS ON MICROWAVE THEORY AND TECHNIQUES.

✠

**Jin Au Kong** (S'65–M'69–SM'74–F'85) is Professor of Electrical Engineering and Chairman of Area IV and Energy and Electromagnetic Systems in the Department of Electrical Engineering and Computer Science at the Massachusetts Institute of Technology, Cambridge, MA. From 1977 to 1980 he served the United Nations as a High-Level Consultant to the Under-Secretary-General on Science and Technology, and as an Interregional Advisor on remote sensing technology for the Department of Technical Cooperation for Development. His research interest is in the area of electromagnetic wave theory and applications. He has published six books and more than 300 refereed journal and conference papers and has supervised more than 100 theses.

Dr. Kong is the Editor for the Wiley series on remote sensing, the Editor-in-Chief of the *Journal of Electromagnetic Waves and Applications* (*JEWA*), and the Chief Editor for the Elsevier book series on Progress in Electromagnetics Research (PIER).

# 射 频 和 天 线 设 计 培 训 课 程 推 荐

易迪拓培训(www.edatop.com)由数名来自于研发第一线的资深工程师发起成立，致力并专注于微波、射频、天线设计研发人才的培养；我们于 2006 年整合合并微波 EDA 网(www.mweda.com)，现已发展成为国内最大的微波射频和天线设计人才培养基地，成功推出多套微波射频以及天线设计经典培训课程和 ADS、HFSS 等专业软件使用培训课程，广受客户好评；并先后与人民邮电出版社、电子工业出版社合作出版了多本专业图书，帮助数万名工程师提升了专业技术能力。客户遍布中兴通讯、研通高频、埃威航电、国人通信等多家国内知名公司，以及台湾工业技术研究院、永业科技、全一电子等多家台湾地区企业。

易迪拓培训课程列表：http://www.edatop.com/peixun/rfe/129.html


## 射频工程师养成培训课程套装

该套装精选了射频专业基础培训课程、射频仿真设计培训课程和射频电路测量培训课程三个类别共 30 门视频培训课程和 3 本图书教材；旨在引领学员全面学习一个射频工程师需要熟悉、理解和掌握的专业知识和研发设计能力。通过套装的学习，能够让学员完全达到和胜任一个合格的射频工程师的要求…

课程网址：http://www.edatop.com/peixun/rfe/110.html

## ADS 学习培训课程套装

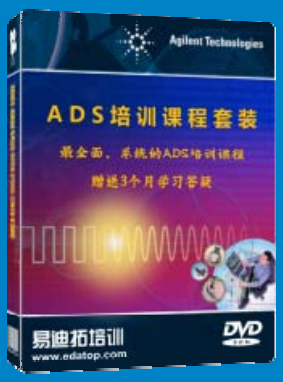


该套装是迄今国内最全面、最权威的 ADS 培训教程，共包含 10 门 ADS 学习培训课程。课程是由具有多年 ADS 使用经验的微波射频与通信系统设计领域资深专家讲解，并多结合设计实例，由浅入深、详细而又全面地讲解了 ADS 在微波射频电路设计、通信系统设计和电磁仿真设计方面的内容。能让您在最短的时间内学会使用 ADS，迅速提升个人技术能力，把 ADS 真正应用到实际研发工作中去，成为 ADS 设计专家...

课程网址： http://www.edatop.com/peixun/ads/13.html

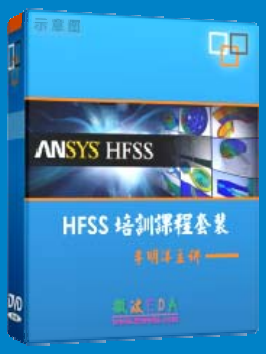


## HFSS 学习培训课程套装

该套课程套装包含了本站全部 HFSS 培训课程，是迄今国内最全面、最专业的 HFSS 培训教程套装，可以帮助您从零开始，全面深入学习 HFSS 的各项功能和在多个方面的工程应用。购买套装，更可超值赠送 3 个月免费学习答疑，随时解答您学习过程中遇到的棘手问题，让您的 HFSS 学习更加轻松顺畅…

课程网址：http://www.edatop.com/peixun/hfss/11.html

## CST 学习培训课程套装


该培训套装由易迪拓培训联合微波 EDA 网共同推出，是最全面、系统、专业的 CST 微波工作室培训课程套装，所有课程都由经验丰富的专家授课，视频教学，可以帮助您从零开始，全面系统地学习 CST 微波工作的各项功能及其在微波射频、天线设计等领域的设计应用。且购买该套装，还可超值赠送 3 个月免费学习答疑…

**课程网址**：http://www.edatop.com/peixun/cst/24.html


## HFSS 天线设计培训课程套装

套装包含 6 门视频课程和 1 本图书，课程从基础讲起，内容由浅入深，理论介绍和实际操作讲解相结合，全面系统的讲解了 HFSS 天线设计的全过程。是国内最全面、最专业的 HFSS 天线设计课程，可以帮助您快速学习掌握如何使用 HFSS 设计天线，让天线设计不再难…

**课程网址**：http://www.edatop.com/peixun/hfss/122.html

## 13.56MHz NFC/RFID 线圈天线设计培训课程套装


套装包含 4 门视频培训课程，培训将 13.56MHz 线圈天线设计原理和仿真设计实践相结合，全面系统地讲解了 13.56MHz 线圈天线的工作原理、设计方法、设计考量以及使用 HFSS 和 CST 仿真分析线圈天线的具体操作，同时还介绍了 13.56MHz 线圈天线匹配电路的设计和调试。通过该套课程的学习，可以帮助您快速学习掌握 13.56MHz 线圈天线及其匹配电路的原理、设计和调试…

**详情浏览**：http://www.edatop.com/peixun/antenna/116.html

## 我们的课程优势：

※ 成立于 2004 年，10 多年丰富的行业经验，

※ 一直致力并专注于微波射频和天线设计工程师的培养，更了解该行业对人才的要求

※ 经验丰富的一线资深工程师讲授，结合实际工程案例，直观、实用、易学

## 联系我们：

※ 易迪拓培训官网：http://www.edatop.com

※ 微波 EDA 网：http://www.mweda.com

※ 官方淘宝店：http://shop36920890.taobao.com